processes

MDPI

Article

Resilience Enhancement Strategy for Power Systems: A Novel Active Response Model

Yanjing Zhang [1], Gang Chen [1], Liang Guo [1], Kunhua Liu [2,*] and Shufang Zhou [3]

[1] Jiangmen Power Supply Bureau, China Southern Power Grid, Jiangmen 529000, China; zhangyj05288@163.com (Y.Z.); chengg_121@163.com (G.C.); guoliang8023@163.com (L.G.)
[2] School of Mechanical and Automotive Engineering, Qingdao University of Technology, Qingdao 266520, China
[3] Institute of Intelligent Manufacturing, Qingdao Huanghai University, Qingdao 266427, China; zhousf@qdhhc.edu.cn
* Correspondence: liukh@qut.edu.cn

Abstract

With the continuously increasing proportion of renewable energy integration, the structure of power grid networks has become increasingly complex. Under extreme weather conditions such as typhoons and hail, faults like line breaks or information disruptions can occur in the power grid, imposing significant burdens and risks on the economic and reliable operation of the power system. However, existing methods still focus on the allocation of human repair teams, with insufficient utilization of flexible resources within the system, resulting in low efficiency in restoring power supply to the power system. To address this challenge, this paper proposes a resilience enhancement strategy for the power system under typhoon scenarios. It leverages active resources on the grid side and fully exploits the flexibility of both the supply and demand sides to enhance the resilience of the power system. Firstly, this paper aims at the economic operation of the power system, taking into account the physical and operational constraints of both the supply and demand sides, including power flow constraints, mobile energy storage system (MESS) transfer constraints, and phase-shifting transformer (PST) regulation constraints. Meanwhile, an improved grasshopper optimization algorithm is introduced to achieve efficient and rapid problem-solving. Finally, the effectiveness and feasibility of the proposed method are demonstrated through validation using an improved IEEE-33 bus test system. Through analysis, the total system load loss was reduced by 75.6%, with the maximum load loss during the typhoon decreasing by 72.4%. The approach enables real-time response to the dynamic impacts of typhoons, swiftly stabilizes load fluctuations, and significantly enhances the resilience of the power system.

Keywords: extreme weather; self-healing restoration strategy; typhoon scenarios; active resources

Check for updates

Academic Editors: Giampaolo Manzolini, Omar Avalos Alvarez, Jorge Gálvez, Primitivo Diaz and Rolando Menchaca-Méndez

Received: 25 February 2026
Revised: 9 April 2026
Accepted: 30 April 2026
Published: 14 May 2026

Copyright: © 2026 by the authors. Licensee MDPI, Basel, Switzerland. This article is an open access article distributed under the terms and conditions of the Creative Commons Attribution (CC BY) license.

1. Introduction

In recent years, the frequent occurrence of low-probability yet high-risk extreme events has severely impacted the safe and stable operation of power systems. Natural disasters such as the ice and snow disaster in southern China in 2008 [1], Hurricane Irma in Florida, the United States, in 2017 [2], and the magnitude-6.4 earthquake that struck off the coast of Yilan County, Taiwan, China, in 2019 [3] have all caused widespread power outages. Additionally, the threat posed by cyberattacks to power systems cannot be overlooked, as

evidenced by the large-scale power outage experienced by users in Ukraine's power grid due to a cyberattack in 2015 [4]. It is evident that extreme natural disasters and man-made cyberattacks expose power systems to various security threats, making it imperative to develop and construct resilient power systems.

Currently, the resilience assessment of distribution networks primarily focuses on two aspects: static resistance capability and dynamic characteristics [5]. Self-healing in power systems refers to the grid's ability to automatically detect and isolate faults when they occur, and swiftly restore power supply to minimize outages. Power system restoration refers to the process of gradually restoring power supply through dispatching and emergency repairs after a blackout or instability occurs, bringing the grid back to its normal operating state. Resilience enhancement in power systems involves strengthening the grid's ability to withstand disturbances, making it less prone to collapse during extreme events. Even if damaged, it can recover quickly, demonstrating a stronger overall capacity to resist risks. Resilience assessment based on static resistance capability reflects the robustness of distribution network infrastructure when subjected to disturbances, serving as a measure of the anti-interference capability of distribution network components [6]. The resilience assessment method for distribution networks based on dynamic characteristics involves simulating disturbances to generate different stages of distribution network topologies and states. It analyzes the operation of the distribution network during the prevention, resistance, and recovery phases, evaluating the network's ability to maintain operation under disturbances and rapidly restore power supply after failures [7]. The pre-disaster prevention phase mainly involves emergency resource allocation, reinforcement of vulnerable components, and emergency maintenance reserves. Pre-disaster emergency resource allocation primarily involves distributing resources based on disaster prediction information to enhance the post-disaster self-healing efficiency of the distribution system [8]. Reference [9] first generates multiple representative extreme disaster scenarios and then establishes a mixed-integer linear optimization model that includes the pre-disaster placement of mobile emergency power sources and repair teams, considering each scenario. Reference [10] develops a bi-level programming model for enhancing the resilience of distribution systems, focusing on meteorological disaster scenarios such as heavy rainfall and considering emergency power sources and energy storage. Reference [11] directly configures energy storage before disasters from a planning perspective to ensure a continuous and reliable power supply to critical loads, constructing a bi-level power restoration optimization model for the siting and sizing of photovoltaic storage systems in distribution networks and dynamic island partitioning. Reference [12] considers electric vehicle battery swap stations as important scheduling resources and establishes a two-stage stochastic-robust capacity optimization and allocation model for battery swap stations, ensuring effective power supply to outage loads while maintaining transportation functionality. Reference [13] establishes a two-stage robust optimization model considering energy storage configuration to obtain the optimal planning scheme that coordinates line reinforcement and energy storage allocation, ensuring uninterrupted power supply to critical loads during disasters and thereby enhancing the resilience of the distribution system.

With the advancement of information and communication technologies, traditional distribution networks have gradually evolved into physical systems for distribution networks, which are deeply coupled with electricity and information [14]. The high degree of integration and interaction between the information domain and the physical domain has brought intelligent conveniences to distribution network operations. However, they have also enabled cyberattacks in the information domain to propagate across domains to the physical domain, thereby increasing operational risks for distribution networks [15]. From the perspective of network topology factors, Reference [16] establishes a risk propagation

model based on complex networks and proposes corresponding risk assessment indicators considering factors such as risk diffusion rates and initial attack points. From the perspective of measuring system resilience, Reference [17] employs the area of system performance loss as an evaluation metric and defines the difference in resilience between normal and faulty communication states as the impact of information networks on the resilience of distribution networks. Reference [18] proposes an evaluation system for quantifying the vulnerability of information systems by combining the probability of cyberattacks and their resulting consequences on physical equipment, aiming to obtain quantified risk values for different distribution terminals and substations. For distribution networks containing high-density distributed generation (DG), Reference [19] proposes a distributed collaborative control mode based on dynamic attack-defense games to achieve a quantitative assessment of the vulnerability of the distribution network. Furthermore, system resilience enhancement strategies can be classified into investment strategies, operational strategies, and restoration strategies based on their attributes. Among them, investment strategies [20,21] such as line reinforcement and the configuration of DG and energy storage improve system resilience by increasing equipment redundancy; their effects are significant, but the costs are relatively high. Operational strategies [22,23], such as distribution network power flow optimization and network reconfiguration, employ mathematical optimization algorithms to intelligently schedule and control existing flexible resources to enhance system resilience; their effects are limited, but they are economically favorable. Restoration strategies [24,25] involve dispatching maintenance personnel to repair damaged infrastructure and restore normal operational conditions. In practical applications, it is necessary to organically combine resilience enhancement measures with different attributes to formulate an optimal comprehensive strategy. Most existing studies construct indicator systems from two aspects: static anti-disturbance capability and dynamic recovery characteristics, covering load recovery rate, voltage stability, power outage loss, network connectivity, and other dimensions [26]. Reference [27] divides distribution system resilience assessment into three stages: prevention, resistance, and recovery, and quantifies the system's ability to maintain power supply and restore power rapidly by simulating the fault evolution process. Reference [28] takes the system performance loss area as an indicator to quantify the impact on distribution system resilience. With the deep integration of the system, the coupled risk of cyberattacks and physical faults has intensified [29], and relevant assessments have begun to consider factors such as attack propagation paths and the importance of vulnerable nodes. However, most studies still adopt an hourly time scale, which makes it difficult to characterize the spatiotemporal non-uniform characteristics of rapidly evolving disasters such as typhoons, and high-resolution dynamic resilience assessment still needs to be improved. The results of the comparison study on widely used methods are as follows (Table 1):

Table 1. Comparison of existing research methods.

Reference	Core Method	Disaster Scenario	Key Resources	Time Resolution	Quantitative Highlights	Limitations
[8]	Two-stage stochastic robust optimization	Rainstorm/ meteorological disasters	MESS/energy storage	1 h	Load recovery rate increased by about 30%	PST not considered, single time scale
[11]	Optical storage planning + island division	Extreme disasters	Photovoltaic/ energy storage	1 h	Improved power supply reliability of key loads	Static configuration, no dynamic dispatch of mobile resources

Table 1. *Cont.*

Reference	Core Method	Disaster Scenario	Key Resources	Time Resolution	Quantitative Highlights	Limitations
[12]	Flexible dispatch + cooperative fault repair	Distribution network faults	Flexible load/rush repair teams	1 h	Economic loss reduced by about 80%	No spatiotemporal characteristics of typhoon wind farm considered
[17]	Performance loss area assessment	Information–physical faults	None	1 h	Quantified information network impact	No active recovery strategy
[18]	Two-stage defense-recovery	Typhoon	DG/energy storage/SOP	1 h	Lost load cost reduced	No phase-shifting transformer, conventional algorithm

The main innovations of this paper include the following two aspects.

(1) For typhoon scenarios, this paper proposes a collaborative optimal scheduling strategy for multi-type flexible emergency resources integrating phase-shifting transformers and mobile energy storage systems, which dynamically depicts the evolution process of typhoon-induced faults, realizes rapid power flow regulation and load recovery during disasters, and makes up for the deficiency that traditional methods are difficult to track the dynamics of disasters.

(2) An improved grasshopper optimization algorithm is proposed in this paper. By optimizing the convergence coefficient, introducing the elite strategy, and Gaussian mutation perturbation, the solution accuracy and convergence speed are improved, which is more suitable for the real-time requirement of rapid resilience enhancement of power systems.

The overall framework of the paper is as follows. First, Section 2 introduces the fault modeling of transmission lines under typhoon disasters and analyzes in detail the impacts of extreme weather conditions on power system components. On this basis, Section 3 establishes a resilience enhancement strategy for power systems by making full use of flexible resources, including MESS and PST. Since the proposed model has nonlinear and non-convex characteristics that are difficult to solve efficiently with traditional commercial solvers, the corresponding solution algorithm is presented in Section 4. In Section 5, a modified IEEE test system is used to demonstrate the effectiveness and feasibility of the proposed method. Finally, Section 6 concludes the whole paper.

2. Fault Modeling of Transmission Lines Under Typhoon Disasters

2.1. Typhoon Disaster Modeling

The new-type power system is dominated by high-proportion new energy, relies on the coordinated interaction of generation-grid–load–storage and intelligent regulation technologies, and features clean low-carbon emissions, safety, flexibility, high efficiency, and intelligence. It can adapt to the randomness and volatility of large-scale renewable energy integration, and is a modern power system that supports the "dual carbon" goal and the construction of a new energy system. Typhoons directly damage components on the transmission grid side of new-type power systems through strong wind pressure, with harmful consequences including tower collapses and line breaks, wind-induced flashovers, and the suspension of foreign objects. Due to the difficulty in obtaining practical engineering data, it is challenging to comprehensively consider these harmful effects. Consequently, most existing studies focus on the impact of typhoons on transmission systems primarily in terms of tower collapses and line breaks. This paper follows this approach and only considers the effects of typhoon disasters on components on the transmission grid side of

new-type power systems. The Batts model can accurately characterize the spatiotemporal variations in key typhoon parameters, including central pressure difference, moving path, and maximum wind speed, and effectively quantify the wind field conditions of power grid components within the typhoon-affected area. It has a mature application basis and reliable calculation accuracy in typhoon disaster-related engineering research. In addition, it can be conveniently combined with the vulnerability functions of transmission lines and towers to calculate failure probabilities, which meets the needs of this paper for quantitative analysis of power system faults under typhoon disasters. Meanwhile, it is compatible with the test system and simulation scenarios adopted in this paper, providing a stable and realistic disaster simulation foundation for the subsequent fault analysis and resilience enhancement strategy research. To quantify the impact of typhoons on transmission system components at different times, the Batts model is employed to simulate the temporal variation process of typhoons.

$$\Delta h(t) = \Delta h(t_{land}) - 0.02[1 + \sin(\varphi - \theta)] \tag{1}$$

$$v_{ground}^{\max}(t) = K\sqrt{\Delta h(t)} \tag{2}$$

$$v_H^{\max}(t) = 0.865 v_{ground}^{\max}(t) + 0.5 v_H(t) \tag{3}$$

In Equations (1)–(3), $\Delta h(t)$ represents the central pressure difference in the typhoon at time t; $\Delta h(t_{land})$ denotes the central pressure difference in the typhoon at the landfall time t_{land}; φ and θ are the angles between the typhoon's direction of travel and the coastline, and the positive north direction, respectively; $v_H(t)$ is the typhoon's forward speed; K is a location coefficient with a value of 6.93. Based on the relative position of the component from the typhoon center, the wind speed at the component's location can be further determined. $v_{ground}^{\max}(t)$ denotes the maximum ground-level wind speed of the typhoon at time t, which is the actual wind speed index directly acting on facilities such as transmission towers and power lines in the power system, and is used to calculate the failure probability of relevant components. $v_H^{\max}(t)$ represents the maximum wind speed of the typhoon itself, which is a core physical parameter describing the intensity of the typhoon, and is used for the simulation and characteristic quantification of the whole typhoon process.

$$v_{comp}(t) = \begin{cases} v_H^{\max}(t) d(t) / R_H^{\max}(t), & d(t) \le R_H^{\max}(t) \\ v_H^{\max}(t) (R_H^{\max}(t)/d(t))^{0.6}, & d(t) > R_H^{\max}(t) \end{cases} \tag{4}$$

In the field of power system resilience and reliability assessment, system components such as transmission towers and power lines are usually regarded as individual components. Here, $v_{comp}(t)$ represents the wind speed at the component's location at time t; $d(t)$ is the relative distance between the typhoon center and the component at time t; $R_H^{\max}(t)$ denotes the radius of maximum wind speed of the typhoon at time t. The formulas for calculating the relative distance and the radius of maximum wind speed are as follows:

$$d(t) = \sqrt{(x_{comp} - x_H(t))^2 + (y_{comp} - y_H(t))^2} \tag{5}$$

$$x_H(t) = x_H(land) + v_H(t) t \cos\delta \tag{6}$$

$$y_H(t) = y_H(land) + v_H(t) t \sin\delta \tag{7}$$

$$R_H^{\max}(t) = e^{(3.859 - 7.7001 * 10^{-5} \Delta h(t)^2)} \tag{8}$$

Here, (x_{comp}, y_{comp}) and $(x_H(t), y_H(t))$ represent the location coordinates of the power grid component and the location coordinates of the typhoon center at time t, respectively; $(x_H(land), y_H(land))$ denotes the location coordinates of the typhoon center at the landfall

time t_{land}; δ is the angle between the typhoon path and the coastline. Typhoon disaster modeling serves as an indispensable physical foundation and prerequisite analysis step for the research on power system resilience enhancement under extreme typhoon scenarios in this paper. By quantitatively characterizing the spatiotemporal evolution of typhoons using the Batts model, the failure probability of transmission lines and towers under typhoon impact can be accurately calculated, and the influence laws and fault mechanisms of disasters on power grid components can be clarified, providing realistic and reasonable fault scenario support for the subsequent construction of the optimal scheduling model for multi-type flexible emergency resources. These model descriptions are used to generate the subsequent typical typhoon scenarios.

2.2. Calculation of Failure Probability for Transmission Lines Under Typhoon Disasters

When studying the impact of typhoons on components of the transmission system, transmission lines are often more susceptible to damage from extreme wind speeds, whereas transformers and generators are less affected. Therefore, this paper only considers the damage scenarios of transmission lines under typhoon disasters. Given that different sections of a transmission line are subjected to varying wind speeds, this paper treats a transmission line as a combination of multiple transmission towers and line segments connected together.

(1) Calculation of Cumulative Failure Probability for Transmission Towers and Line Segments

This paper employs a vulnerability function to calculate the failure probability of transmission towers under typhoon disasters. The cumulative failure probability of a tower over the duration of a typhoon can be calculated using the following formula:

$$\mu_{l,m}(t_i) = \begin{cases} 0, & v_{l,m}(t_i) \in [0, v_{tower}^{design}] \\ e^{0.2[v_{l,m}(t_i) - 2v_{tower}^{design}]}, & v_{l,m}(t_i) \in (v_{tower}^{design}, 2v_{tower}^{design}) \\ 1, & v_{l,m}(t_i) \in [2v_{tower}^{design}, \infty) \end{cases} \tag{9}$$

$$p_{l,m} = 1 - \exp\left[- \sum_{i=0}^{NT-1} \frac{\mu_{l,m}(t_i)}{1 - \mu_{l,m}(t_i)} \Delta t \right] \tag{10}$$

Here, $\mu_{l,m}(t_i)$ represents the failure probability of the m-th tower on transmission line l at time t_i; $v_{l,m}(t_i)$ denotes the wind speed at the m-th tower on transmission line l at time t_i; v_{tower}^{design} is the design wind speed for the tower, with a value of 35 m/s; Δt is the unit time interval, taken as 1 h in this paper; NT is the total number of time intervals. Equation (9) is established based on the vulnerability characteristics of transmission towers under typhoon impact. By cumulatively calculating the failure probability of the tower corresponding to the wind speed at different time instants in the time dimension, it can fully reflect the physical mechanism of gradual cumulative damage and eventual failure of the tower during the continuous influence of a typhoon. This model form is derived from the common research methods in the field of typhoon disaster risk assessment for power systems, which can reasonably characterize the quantitative relationship between wind speed and structural failure probability. The parameter selection is determined according to the general design standards of transmission towers and is consistent with the mature disaster loss analysis ideas in the industry. It has sufficient theoretical basis and engineering applicability, thus ensuring the correctness and rationality of the calculation method and model structure.

(2) The cumulative failure probability of a transmission line segment over the duration of a typhoon can be calculated using the following formula:

$$\mu_{l,n}(t_i) = \exp[11 * \frac{v_{l,n}(t_i)}{v_{line}^{design}} - 18]\Delta l \tag{11}$$

$$p_{l,n} = 1 - \exp\left[-\sum_{i=0}^{NT-1} \mu_{l,n}(t_i)\Delta t\right] \tag{12}$$

Here, $\mu_{l,n}(t_i)$ represents the failure probability of the n-th line segment on transmission line l at time t_i; $v_{l,n}(t_i)$ denotes the wind speed of the n-th line segment on transmission line l at time t_i; Δl represents the length of the line segment between adjacent towers, with a value of 350 m; v_{line}^{design} is the design wind speed for the line, taken as 30 m/s in this paper.

The cumulative failure probability of transmission line l over the duration of a typhoon can be calculated using (13).

$$P_l = 1 - \prod_{1}^{M}(1 - p_{l,m})\prod_{1}^{L}(1 - p_{l,n}) \tag{13}$$

Here, M and L represent the total number of towers and line segments for the l-th transmission line, respectively. To verify the effectiveness of the proposed fault model, the widely recognized Batts wind field model for typhoon disaster research in power systems is first adopted. Parameters such as central pressure difference, maximum wind speed radius, and movement path are used to fit the measured characteristics of typical typhoons over the southeastern coastal areas, ensuring that the wind field input conforms to real disaster laws. Second, the wind speed-failure cumulative vulnerability function widely used in the power industry is adopted for the failure probability of transmission towers and lines. Parameters, including tower design wind speed of 35 m/s and conductor design wind speed of 30 m/s, are calibrated against power engineering design standards to ensure reasonable values and clear physical significance of the failure probability curves. Finally, the time-varying wind speed output from the typhoon model is substituted into the failure probability model to obtain component fault results at different time periods. Through distribution network power flow calculation, load recovery optimization, and comparison of resilience indicators, it is verified that the model output is logically consistent with the system response and shows a reasonable trend. Equation (10) is the formula for calculating the instantaneous failure probability of a transmission tower at any moment during a typhoon. It characterizes the failure possibility of a single tower under the current wind speed and serves as the core calculation unit for the cumulative failure probability in Equation (9) within each time step. Equation (12) is the formula for calculating the instantaneous failure probability of a transmission line segment at any moment during a typhoon. It characterizes the failure possibility of a unit line segment under the current wind speed and provides a time-by-time calculation basis for the cumulative failure probability of the line segment in Equation (11). Together with Equations (9) and (11) respectively, the two form an instantaneous-cumulative two-layer failure probability model, which fully describes the failure evolution law of transmission towers and line segments throughout the entire typhoon process.

3. Optimization and Scheduling Strategy for Multi-Type Flexible Emergency Resources

3.1. Phase-Shifting Transformer Response Model

Considering the integration of photovoltaic systems and energy storage into the distribution network, prior to a disaster, the distribution network is powered by the superior main grid. During the disaster, line components may suffer damage within a short period, leading to the distribution network losing power supply from the main grid and

resulting in several faulted lines. The phase-shifting transformer (PST) alters the magnitude and direction of power flow in transmission lines by changing the phase angle of the voltage at its two ends. Before the installation of a PST, the active power transmitted by line ij is given by

$$P_{ij} = \frac{U_i U_j}{X_{ij}} \sin(\theta_i - \theta_j) \tag{14}$$

The schematic representation of the PST in the system is shown in Figure 1.

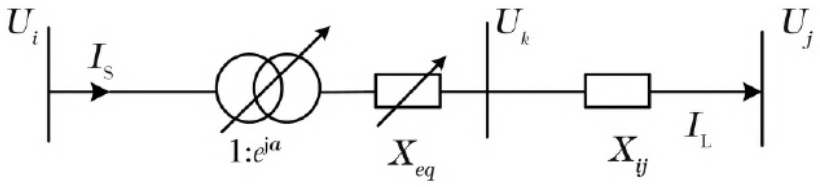

Figure 1. The schematic representation of the PST.

After incorporating the PST, the active power transmitted by line ij is given by (15).

$$P_{ij} = \frac{U_i U_j}{X_{ij} + X_{eq}} \sin(\theta_i - \theta_j + a_i) \tag{15}$$

Here, P_{ij} represents the active power transmitted through branch ij; U_i, θ_i, U_j and θ_j are the voltage magnitude and phase angle at node i, and the voltage magnitude and phase angle at node j, respectively. X_{eq} is the equivalent reactance of the PST; a_i is the phase-shifting angle; and X_{ij} is the equivalent reactance of the connected line. As depicted in Figure 1, installing a PST between lines alters the phase difference between the lines by an angle of a_i, thereby changing the magnitude and direction of power flow in the lines and enabling power distribution and load balancing among different lines. Incorporating the PST into tie lines not only ensures the safety of the reconfiguration process but also significantly reduces the loop-closing current, enhancing the safety margin of loop-closing operations and thus enabling rapid power supply to loads after a disaster. In the model proposed in this paper, the decision variable related to PSTs is the phase-shift angle optimization. The installation locations of PSTs are not treated as decision variables in this paper; instead, PSTs are mainly installed at key nodes with heavy power loads. The optimization of the phase-shift angle is embedded in the scheduling model as a key variable. In other words, the power flow distribution in the power flow constraints is affected by PSTs. It should be noted that the adjustment range of the phase-shift angle is limited, which is set to -10° to 10° in this paper.

3.2. Objective Function and Constraints

The objective function of this paper is to minimize the load shedding amount in the power grid over the scheduling period, as shown in (16).

$$obj = \min \sum_{t=1}^{T} \sum_{i=1}^{I} \Delta P_{i,t}^{load} \tag{16}$$

Here, T represents the total scheduling period, I denotes the total number of nodes, and $\Delta P_{i,t}^{load}$ represents the load shedding amount at node i at time t.

MESS is a device that can move flexibly via the transportation network and has the functions of energy storage and release. It can store electric energy in the form of chemical energy and convert it back to electric energy for output when needed. It can be applied to various scenarios such as emergency power supply, power peak shaving,

outdoor operation, and electric vehicle energy replenishment, effectively improving the flexibility and reliability of energy utilization. When the MESS moves among various charging stations to coordinate load restoration in the distribution network, the following constraints (17)–(19) must be satisfied:

$$\sum_{n^{tn} \in N^{TN}} u^{nd}_{m,n^{tn},t} \leq 1, \forall m \in M, \forall n^{tn} \in N^{TN}_{CS}, \forall t \in T \tag{17}$$

$$\sum_{m \in M} u^{nd}_{m,n^{tn},t} \leq K^{cap}_{n^{tn}}, \forall n^{tn} \in N^{TN}_{CS}, \forall m \in M, \forall t \in T \tag{18}$$

$$\sum_{\tau=t}^{\min(t+T^{M}_{bp,t})} u^{nd}_{m,p,t} \leq (1 - u^{nd}_{m,b,t}) \bullet \min(T^{M}_{bp,t}, T - t), \forall b \neq p \in N^{TN} \tag{19}$$

Here, N^{TN} and N^{TN}_{CS} represent the sets of transportation network nodes, and charging station nodes on the transportation network side, respectively; $u^{nd}_{m,n^{tn},t}$ is a binary variable that equals 1 if the MESS is located at a transportation network node n^{tn} at time t, and 0 otherwise; $K^{cap}_{n^{tn}}$ denotes the maximum number of MESSs allowed to access a charging station node, M represents the number of MESSs. Constraints (17)–(18) impose restrictions on the location of the MESS within the transportation network. Constraint (19) is the MESS mobility constraint, where $T^{M}_{bp,t}$ represents the time required for the MESS to move between transportation network nodes, influenced by road conditions.

After the MESS arrives at the target charging station at time t, its power scheduling must satisfy the following constraints:

$$0 \leq P^{mess,c}_{m,t} \leq cp^{mess}_{m,t} P^{\max}_{m} \tag{20}$$

$$0 \leq P^{mess,d}_{m,t} \leq dp^{mess}_{m,t} P^{\max}_{m} \tag{21}$$

$$0 \leq Q^{mess,d}_{m,t} \leq \sum_{n^{tn} \in N^{TN}_{CS}} u^{nd}_{m,n^{tn},t} Q^{\max}_{m} \tag{22}$$

$$cp^{mess}_{m,t} + dp^{mess}_{m,t} \leq \sum_{n^{tn} \in N^{TN}_{CS}} u^{nd}_{m,n^{tn},t} \tag{23}$$

$$S_{m,t} = S_{m,t-1} + (\eta^{c}_{m} P^{mess,c}_{m,t} - \frac{P^{mess,d}_{m,t}}{\eta^{d}_{m}}) \bullet \Delta t \tag{24}$$

$$\underline{S}_{m} \leq S_{m,t} \leq \overline{S}_{m} \tag{25}$$

Here, $cp^{mess}_{m,t}$ and $dp^{mess}_{m,t}$ are the charge and discharge state variables of the MESS, respectively; $P^{mess,c}_{m,t}$, $P^{mess,d}_{m,t}$ and $Q^{mess,d}_{m,t}$ represent the active charging power, active discharging power, and reactive power, respectively; $P^{\max}_{m}$, and $Q^{\max}_{m}$ denote the upper limits of active charging/discharging power and reactive power, respectively; $S_{m,t}$ is the current state of charge (SOC) value; η^{c}_{m} and η^{d}_{m} are the charging and discharging efficiency coefficients, respectively; and $\underline{S}_{m}$ and $\overline{S}_{m}$ are the upper and lower limits of the SOC value, respectively. Other conventional constraints are detailed in Appendix A.

4. Solution Strategy Based on an Improved Grasshopper Optimization Algorithm

4.1. Basic Principles of the Grasshopper Optimization Algorithm

The grasshopper optimization algorithm (GOA) simulates the foraging behavior of grasshoppers in nature. It divides the search space through repulsive and attractive forces among grasshoppers to seek the optimal solution. The multi-flexible resource collaborative

optimization problem solved in this paper—including phase-shifting transformer regulation, mobile energy storage relocation, and distribution network reconfiguration—is a complex optimization problem with coupled discrete and continuous variables, as well as nonlinear and non-convex characteristics. Traditional convex optimization and linear programming methods can hardly solve it effectively. As a typical swarm intelligence optimization algorithm, the grasshopper optimization algorithm has strong global search ability and good adaptability in handling complex nonlinear constraints, enabling efficient optimization in multi-dimensional and non-convex solution spaces. Therefore, this algorithm is adopted as the solution tool, which can better match the complex characteristics of the model in this paper and the demand for a fast solution.

The optimization process of GOA comprises two stages: exploration and exploitation. The exploration stage is analogous to the adult phase of grasshoppers, during which they possess the ability to fly and can search for potential high-quality solutions across a vast space. Conversely, the exploitation stage resembles the egg and nymph stages of grasshoppers, where they move slowly with small steps, and the algorithm primarily conducts local searches to accelerate convergence. GOA updates the positions of grasshoppers using the following formula:

$$x_{d,i} = c^2 \sum_{j=1, j\neq i}^{N} \frac{b_{u,d} - b_{l,d}}{2} s\left(\left|x_{d,j} - x_{d,i}\right|\right) \frac{x_j - x_i}{D_{ij}} + T_d \tag{26}$$

Here, $x_{d,i}$ represents the position of the i-th grasshopper in the d-th dimension; N is the population size; $b_{u,d}$ and $b_{l,d}$ are the upper and lower bounds, respectively, of the d-th dimension; T_d is the current best solution in the d-th dimension; D_{ij} denotes the distance between the i-th and j-th grasshoppers, given by $D_{ij} = \left|x_j - x_i\right|$; the s function is expressed as $s(r) = e^{-\frac{r}{k}} f - e^{-r}$, where the intensity of attraction f = 0.5 and the range of attraction k = 1.5.

4.2. Algorithm Improvement and Enhancement

In the GOA, the position update coefficient c determines the search range of the algorithm. We have improved the parameter c such that it decreases more slowly in the early iterations, thereby avoiding the issue of local optima caused by a rapid decrease in c during the initial stages. Conversely, in the later iterations, c decreases more rapidly to prevent slow convergence resulting from an overly gradual reduction in c.

$$c = \begin{cases} \left[(c_{\max} - c_{\min}) \cos\left(\frac{\pi l}{2L}\right)\right]^3, 0 < l < 0.3L \\ c_{\max} - l\frac{c_{\max} - c_{\min}}{L}, 0.3L \leq l \leq 0.7L \\ c_{\max} - \left(\sin\left(\frac{\pi l}{2L}\right)\right)^3, l > 0.7L \end{cases} \tag{27}$$

Here, l represents the current iteration number; L denotes the maximum number of iterations; and $c_{\max}$ = 1, whereas $c_{\min}$ = 0.00001.

The ant lion optimizer exhibits excellent convergence and the ability to escape local optima. By introducing the elite strategy from this algorithm, we enhance the performance of the grasshopper optimization algorithm.

$$x_{d,l} = \frac{R_{l,A} + R_{l,E}}{2} \tag{28}$$

Here, $x_{d,l}$ represents the position of the grasshopper in the d-th dimension during the l-th iteration; $R_{l,A}$ denotes the position of the grasshopper selected by roulette wheel

selection during the l-th iteration; $R_{l,E}$ is the position of the elite grasshopper, i.e., the global best solution, during the l-th iteration.

Gaussian mutation perturbation is randomly introduced to the population to reduce the likelihood of the algorithm getting trapped in local optima. The perturbation formula is as follows:

$$x_{l+1,i} = \frac{1}{\sqrt{2\pi}\sigma} e^{-\frac{(R_{l,E}-x_{l,i})^2}{2\sigma^2}} x_{l,i} \tag{29}$$

Here, σ represents the Gaussian mutation coefficient, which is set to 0.7 in this paper; $x_{l,i}$ denotes the position of the grasshopper during the l-th iteration.

To gain a better understanding, the solution flow chart of IGOA is given in Figure 2.

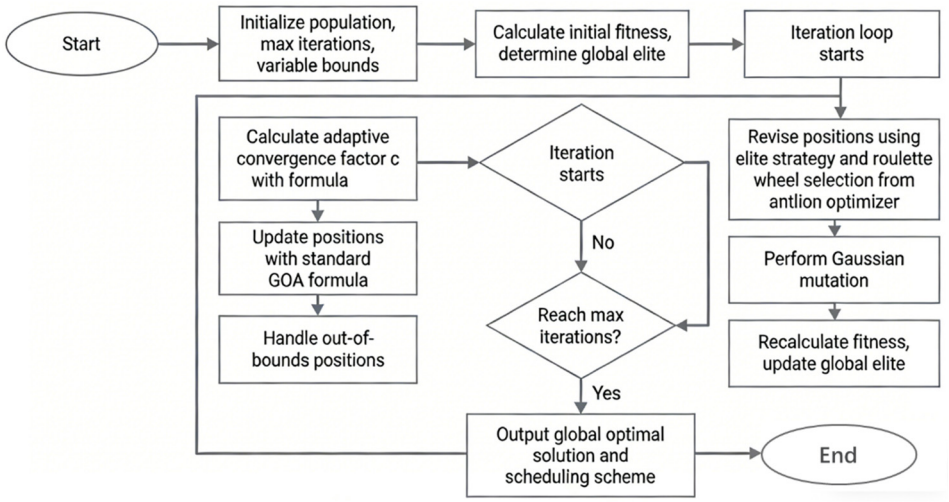

Figure 2. Solution flow chart of IGOA.

5. Case Study

To verify the effectiveness of the method proposed in this paper, an improved IEEE–33 bus test system was employed for analysis. The network topology of this test system is shown in Figure 3 below. As depicted in the figure, the test system is affected by a typhoon, and the typhoon's trajectory continuously shifts and changes over different time periods. Mobile energy storage access points are installed at nodes 5, 9, 17, 20, 24, and 32 within the system, while distributed wind power and photovoltaic power are respectively installed at node 21 and node 16. The key parameter settings of the typhoon model used in the simulation of this paper are as follows: the typhoon central pressure drop is 40 hPa, the radius of maximum wind speed is 30 km, the angle between the typhoon moving path and the coastline is set to 45°, the typhoon moving speed is 18 m/s, the position coefficient is 6.93, the tower design wind speed is 35 m/s, the line design wind speed is 30 m/s, and the time resolution is 15 min. The parameters of the tower and line failure probability model can be referred to References [30,31]. Each MESS unit is rated at 1 MWh/0.5 MW. The average driving speed on urban roads is 30 km/h, with a maximum continuous driving range of 80 km per single dispatch. The one-way travel time between nodes is quantified as 15 min per 10 km, and the travel time conversion factor under restricted road conditions after a typhoon disaster is 1.2. The maximum charging power of the MESS is 250 kW with a charging efficiency of 0.95. It takes approximately 2.5 h to charge from 20% SOC to 90% SOC. The maximum discharging power is 500 kW, which can meet the emergency power supply demand of critical loads. The system base capacity is 10 MVA, and the base voltage is 12.66 kV. The network consists of 33 buses and 37 branches, all operating in radial mode. The total active power of node loads is approximately 3.715 MW, and the total reactive power is about 2.300 Mvar. The upper limit of the rated line capacity is 2.0 MVA,

and the rated current meets the requirements of power flow transfer and flexible dispatch under typhoon scenarios. The PST is installed on key tie branches with an equivalent reactance of 0.05 p.u. and a phase-shift range of −15°~+15°, enabling closed-loop secure reconfiguration and precise power flow regulation.

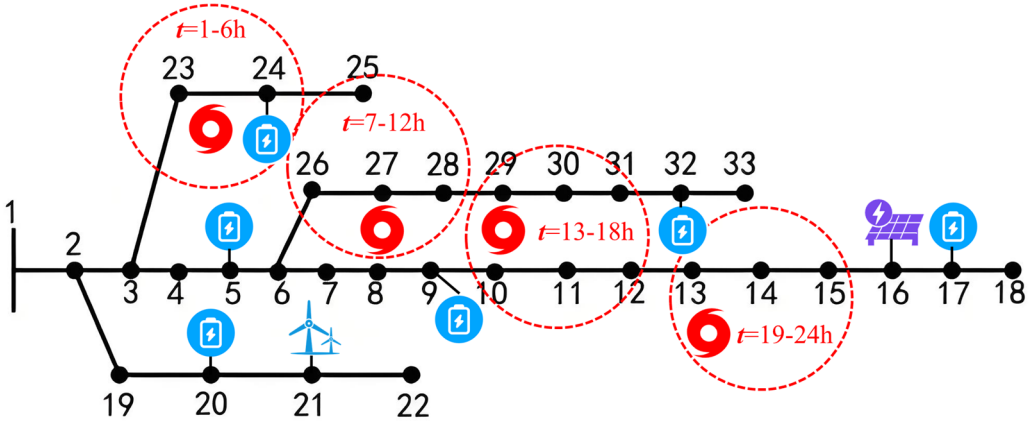

Figure 3. Topology structure of the improved IEEE-33-node test system.

After a typhoon passes through the distribution network, it leads to an increased fault rate, as illustrated in Figure 4 below.

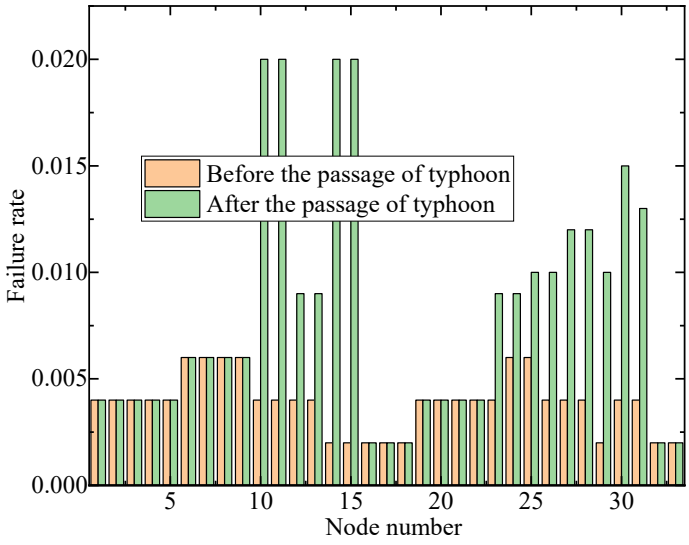

Figure 4. Comparison of fault rates before and after typhoon passage.

Observing Figure 4 above, it can be found that the fault rates of nodes, including towers and transmission lines, within the area affected by the typhoon significantly increase. The strong winds brought by the typhoon exert tremendous lateral pressure on the towers, potentially causing them to tilt, deform, or even collapse. Meanwhile, the strong winds may also blow foreign objects to strike the towers, resulting in structural damage. Under the influence of strong winds, the transmission lines will swing and gallop violently, leading to a reduction in the safety distance between conductors and towers. This makes it prone to faults such as inter-phase short circuits or ground discharges. Additionally, the heavy rain brought by the typhoon may cause the surface of line insulators to become damp with dirt, reducing their insulation performance and increasing the risk of flashover, thereby significantly raising the fault rates of towers and transmission lines.

After the response of flexible resources, the resilience of the power system can be significantly enhanced. Figures 5 and 6 below respectively illustrate the response situations of the MESS and PSTs.

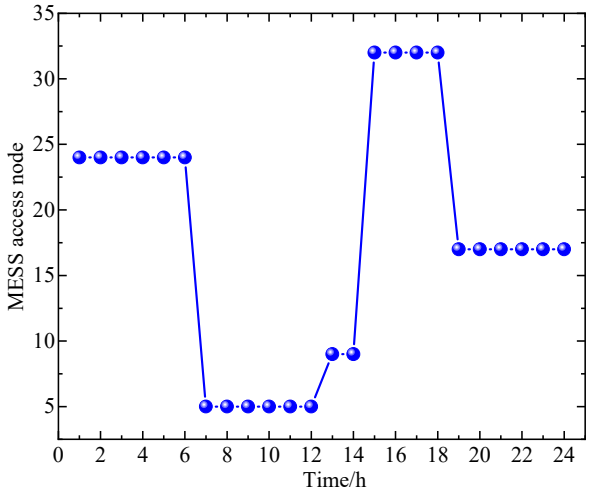

Figure 5. Movement trajectory of MESS.

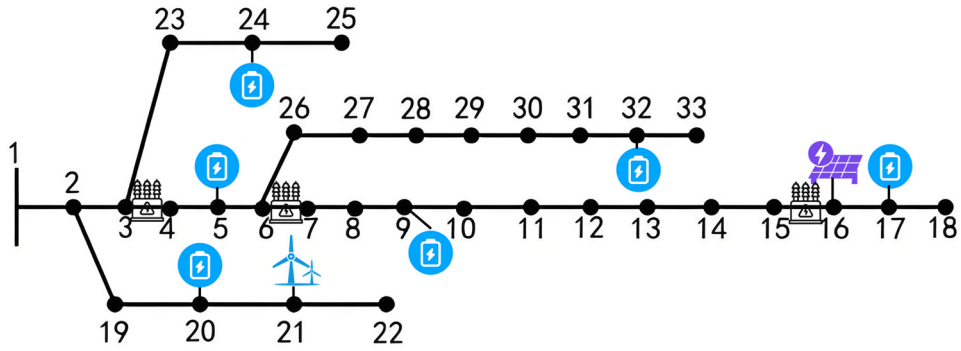

Figure 6. Installation location of PSTs.

Upon observing Figure 5, it can be seen that under typhoon disasters, mobile energy storage vehicles follow the movement of the typhoon. Typhoon passage is often accompanied by severe damage to power grid facilities, resulting in localized or widespread power outages. Leveraging their flexibility and rapid deployment capabilities, mobile energy storage vehicles can swiftly arrive at disaster-stricken areas to provide uninterrupted power support for critical loads such as hospitals and emergency command centers, ensuring their basic operation. Simultaneously, they can serve as temporary power sources during power grid restoration, alleviating the contradiction between power supply and demand, accelerating the post-disaster reconstruction process, and effectively smoothing out grid load fluctuations caused by typhoons through the charging and discharging regulation of the energy storage system, thereby enhancing the stability and resilience of the power system. In Figure 6, under typhoon disasters, installing PSTs at critical load nodes and central nodes can effectively regulate the power distribution within the power system. By altering the voltage phase difference to optimize power flow direction, it prevents chain outages triggered by line faults or local overloads caused by typhoons. Meanwhile, it enhances the tolerance of critical nodes to voltage fluctuations, ensuring the power supply quality for important loads even when the power grid structure is damaged, and improving the system's disaster resilience and recovery capabilities under extreme conditions.

Figure 7 further illustrates the system load loss before and after optimization. There is a notable reduction in system load loss following the optimization. By introducing flexi-

ble emergency resources such as phase-shifting transformers and mobile energy storage vehicles, and implementing optimized dispatching based on an improved grasshopper optimization algorithm, intelligent regulation of power flow and rapid load restoration in the power system have been achieved. The phase-shifting transformers optimize power distribution by adjusting the voltage phase difference, preventing line overloads and cascading failures. Meanwhile, mobile energy storage vehicles, with their flexible deployment capabilities, track power supply demands in real-time as the typhoon moves, providing uninterrupted power support to critical loads while smoothing out load fluctuations. This effectively reduces the amount of load shedding caused by equipment damage and supply-demand imbalances under extreme weather conditions, significantly enhancing the resilience and recovery capacity of the power system.

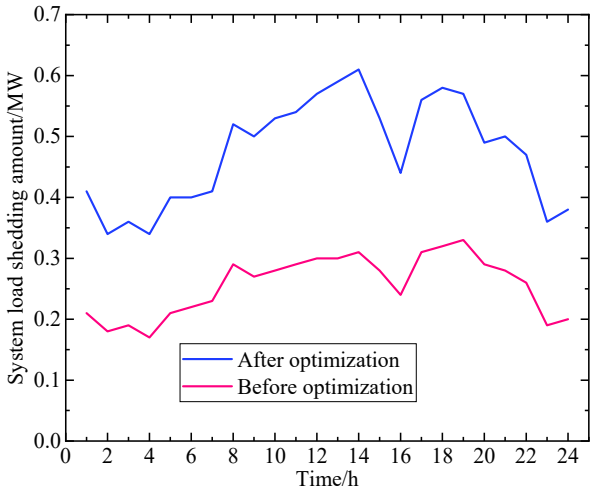

Figure 7. System load loss before and after optimization.

Considering that the time scale of real-time dispatch in modern power systems is 10–15 min, this paper further analyzes the load loss of the system under a short time resolution, as shown in Figure 8 below.

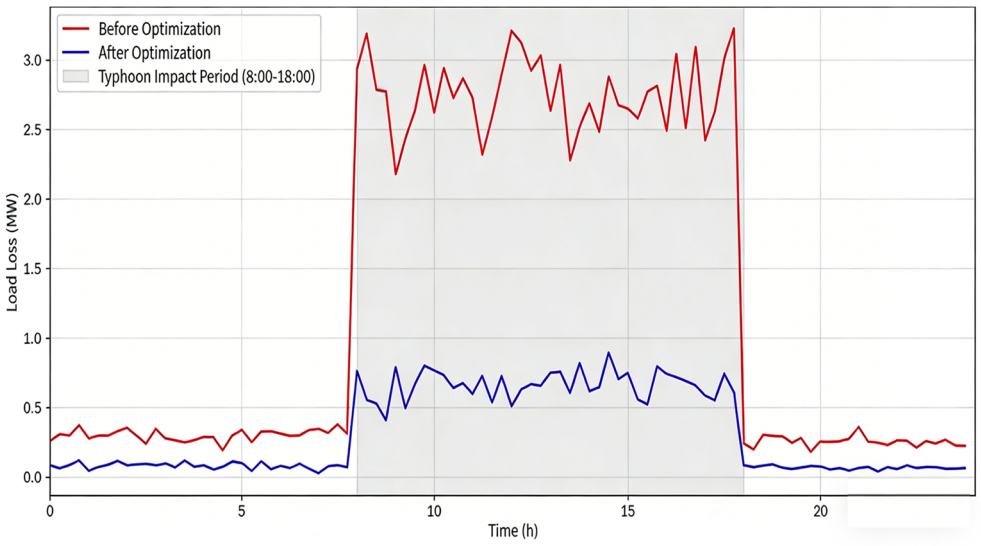

Figure 8. Load loss of the system under a 15 min resolution.

MESS dynamically optimizes its deployment location every 15 min by tracking typhoon tracks. The power supply response delay at critical nodes is less than 15 min, ensuring an uninterrupted power supply for important loads. As a result, it can smooth

out power grid fluctuations caused by typhoons in real time, improve the recovery speed by four times, reduce the total system load loss by 75.6%, and decrease the maximum load loss during typhoons by 72.4%. The proposed method can respond to the dynamic impacts of typhoons in real time, rapidly suppress load fluctuations, and significantly enhance the resilience of power systems.

The tests were conducted on an Intel Core i7-12700H processor (2.3 GHz, 16 GB RAM) using MATLAB R2022b. The maximum number of iterations is set to 100, and the population size is 30. The scheduling objective is to minimize load shedding. The computational efficiency of different algorithms is shown in Table 2, and their convergence curves are illustrated in Figure 9.

Table 2. Computational efficiency among different algorithms.

Algorithm	Average Calculation Time/s	Speed Improvement Compared with Traditional GOA
Traditional GOA	21.7	—
PSO	18.3	+15.7%
GA	26.1	−14.7%
Greedy Algorithm	19.7	+9.22%
The Proposed Method	12.4	+42.9%

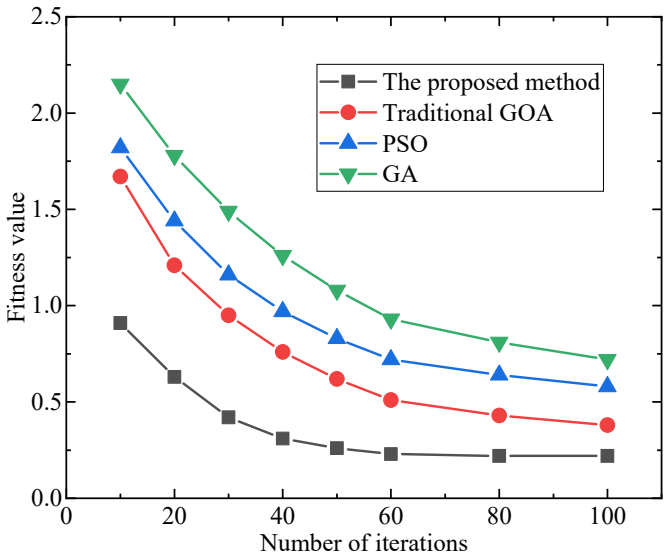

Figure 9. Convergence curves of different algorithms.

It can be observed from the above figure that the improved GOA exhibits the fastest decline in its convergence curve, converging significantly at 30 iterations and fully converging at 60 iterations. In contrast, the traditional GOA shows a slow decline in the middle stage with ordinary convergence accuracy, while PSO and GA decline gently and tend to stagnate in the later stage. For meta-heuristic algorithm parameters such as the Gaussian mutation coefficient, the control variable method combined with orthogonal experiments was adopted in the parameter determination stage of this paper. Taking the optimization accuracy, convergence speed and computing time of the improved GOA as comprehensive evaluation indicators, multiple sets of comparative tests were carried out on key parameters, including the Gaussian mutation coefficient, population size and maximum number of iterations. Finally, the parameter combination with the optimal comprehensive performance in the test system was selected as the default parameter of the model, where the Gaussian mutation coefficient is set to 0.2. This value can enhance the global search ability of the algorithm through moderate mutation disturbance, effectively avoiding the

defect that the standard GOA is easy to fall into a local optimum, without damaging the convergence stability of the algorithm due to excessive mutation amplitude. To verify the effectiveness of parameter selection, additional comparative tests with different parameter values were conducted in the case analysis. The results show that the selected parameter combination can stably output the optimal scheduling scheme under different typhoon fault scenarios. Compared with other parameter values, it can reduce the load shedding amount by 8.7% on average and decrease the convergence iteration number by 12.3%.

In fact, typhoons can significantly impact power supply-side output and load-side demand through factors like strong winds, rainfall, and line outages. It is difficult to truly reflect the operational risks of the system and the robustness of dispatching strategies by solely using deterministic modeling. Therefore, based on the benchmark operating conditions, this paper sets up four scenarios with source–load fluctuation ranges of ±5%, ±10%, ±15%, and ±20%, respectively, and compares the system load loss under deterministic optimization methods and optimization methods that account for uncertainties, as shown in Figure 10 below. It should be noted that a box-type robust model is adopted for the uncertainty fluctuation range here.

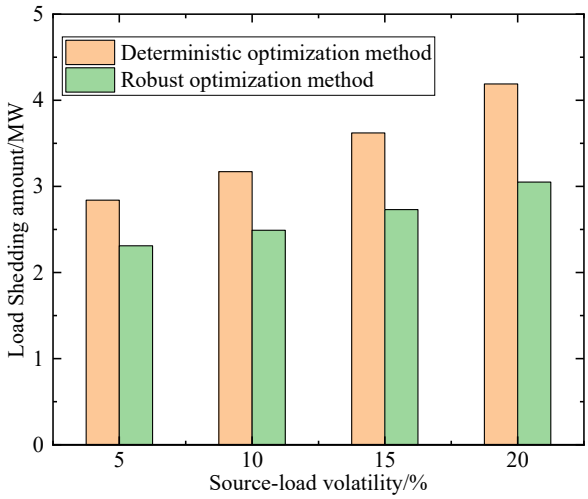

Figure 10. Comparison of system load loss under deterministic and uncertainty optimization.

As the uncertainty fluctuation range of source and load gradually increases from ±5% to ±20%, the load loss under deterministic optimization rises from 2.84 MW to 4.19 MW. The load loss under uncertainty optimization also exhibits an upward trend, indicating that the stronger the source–load fluctuations caused by typhoons, the tighter the power balance constraints in the distribution network become, the more difficult fault restoration becomes, and the load loss level increases significantly as a result. Under various fluctuation scenarios, the load loss obtained through deterministic optimization is consistently significantly higher than that obtained through uncertainty optimization. This is because the deterministic method makes decisions based solely on a single, fixed operating condition and cannot adapt to random fluctuations in source and load. It is prone to issues such as underestimating power deficits and adopting conservative restoration strategies, leading to an underestimation of load loss and overly optimistic resilience assessment results.

To intuitively demonstrate the effectiveness of the scheduling decisions, various resilience indicators are selected for analysis, including the System Average Interruption Duration Index (SAIDI), System Average Interruption Frequency Index (SAIFI), average load recovery time, and critical load recovery percentage. The detailed results are presented in Table 3 below.

Table 3. Comparison and analysis of key resilience indicator values.

Resilience Indicator	No optimization Strategy	Traditional GOA	The Proposed Method
SAIDI (h/customer)	8.26	4.13	1.97
SAIFI (interruptions/customer·year)	1.28	0.74	0.39
Average load recovery time (min)	115	62	28
Critical load recovery percentage (%)	58.2	83.6	97.8

It can be seen from the resilience indicators in Table 3 that the rapid self-healing recovery strategy proposed in this paper can significantly improve the operational resilience of distribution networks under typhoon disasters. Compared with the non-optimized scenario, after adopting the IGOA-based coordinated dispatch of phase-shifting transformers and mobile energy storage systems, the SAIDI is reduced to 1.97 h/customer, a decrease of 76.1%; the SAIFI is reduced to 0.39 interruptions/customer·year, a decrease of 69.5%; the average load recovery time is shortened to 28 min, an improvement of 75.7%; and the critical load recovery rate reaches 97.8%, which effectively guarantees the uninterrupted power supply of important loads. All indicators fully demonstrate that the proposed method can respond to faults quickly, regulate power flow accurately, and restore power supply efficiently, greatly enhancing the disturbance resistance and rapid recovery capability of the power system under extreme typhoon scenarios, which verifies the effectiveness and engineering practicability of the strategy. Throughout the typhoon event, this study adopts typical road traffic parameters for emergency repair of urban distribution networks, sets road traffic reduction coefficients under typhoon influence, and performs rolling scheduling on a 15 min high-resolution time scale, ensuring the rationality and feasibility of travel time, road capacity, and charging scheduling arrangements for MESS. Among them, travel time is calculated based on actual road network distances and average driving speeds, and a traffic capacity correction factor is introduced to account for road blockages caused by typhoons. Charging scheduling is optimally allocated in strict accordance with upper and lower limits of energy storage SOC, charge/discharge power constraints, and real-time load demands. All assumed parameters are derived from engineering practice and the relevant literature standards. Combined with the power flow regulation support of phase-shifting transformers, it is ensured that MESS can arrive on time, supply power reliably, and charge/discharge safely during the dynamic evolution of the typhoon. The overall scheduling scheme meets the requirements of real-time performance and feasibility.

To demonstrate the wide applicability of the proposed method in a larger-scale test system, the IEEE 118-bus test system is adopted for further analysis, whose topology is shown in Figure 11. The system consists of 118 buses, 186 branches, and 91 load buses, with tie switches and network reconfiguration capabilities. The typhoon scenario, fault model, algorithm parameters, and resilience indicators are kept consistent with those in the original IEEE 33-bus case to ensure fair comparison. The benchmark capacity of the test system is 100 MVA; the base voltage is 135 kV/33 kV; the total active load is 113.6 MW; the total reactive load is 77.2 MVAr; there are 18 key load buses; and PSTs are installed on 12 key tie branches.

To clarify the respective effects of MESS and PST on system resilience improvement, four comparison schemes are designed, whose performances are shown in Table 4.

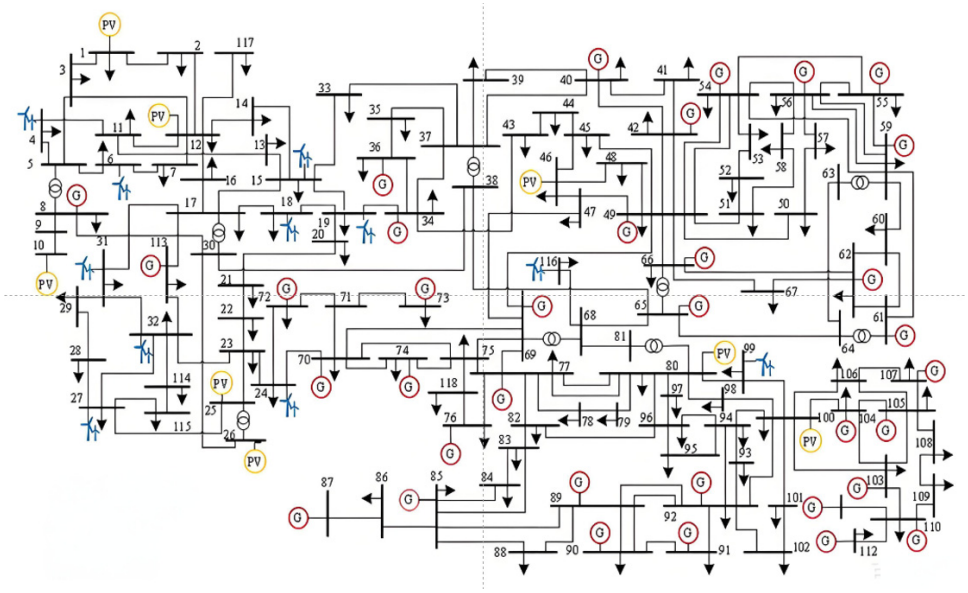

Figure 11. Topology of the IEEE 118-bus system.

Table 4. Comparison of system resilience indicators under different schemes.

Resilience Indicators	Scheme 0	Scheme A	Scheme B	Scheme C
SAIDI (hours per customer)	9.34	5.72	3.18	1.82
SAIFI (interruptions per customer per year)	1.42	0.96	0.58	0.35
Average load restoration time (minutes)	128	76	42	25
Key load recovery rate (%)	54.7	78.3	89.5	98.2
Total load loss reduction range	—	38.8%	65.9%	80.5%

Scheme 0: No optimization (baseline scenario);

Scheme A: PST regulation only;

Scheme B: MESS scheduling only;

Scheme C: Proposed IGOA algorithm + coordinated optimization of PST and MESS.

PSTs accurately optimize power flow distribution by adjusting voltage phase angles, alleviating branch overloads, and suppressing the propagation of cascading failures. They mainly improve voltage stability, power flow balance, and the ability to resist cascading faults. In the IEEE 118 system, PSTs alone can reduce load loss by 38.8% and increase the key load recovery rate from 54.7% to 78.3%. Their advantages include fast response, no movement required, and suitability for global power flow optimization. MESS provides emergency power supply for key loads and smooths load fluctuations through rapid movement and local charging/discharging. It mainly improves post-disaster power supply capability, load restoration speed, and the ability to guarantee key load supply. In the IEEE 118 system, MESS alone can reduce load loss by 65.9% and shorten the average restoration time from 128 min to 42 min. MESS features strong mobility and a direct power supply guarantee, making it suitable for dynamic tracking and emergency power supply during typhoons. PSTs stabilize power flow and prevent overloads, while MESS ensures key load supply and rapid restoration. Through their coordination, the total load loss is reduced by 80.5%, the key load recovery rate reaches 98.2%, and the restoration time is only 25 min, which is far superior to using either device alone.

A comparison of the computational efficiency and solution quality among different algorithms is shown in Table 5 below.

Table 5. Computational efficiency and solution quality among different algorithms.

Algorithm	Average Computation Time (s)	Minimum Load Loss (MW)	Number of Convergence Iterations	Efficiency Improvement Compared with Traditional GOA
GOA	47.2	28.6	112	—
PSO	41.5	25.1	98	12.1%
GA	52.8	30.3	126	−11.9%
IGOA	26.8	19.4	63	43.2%

The load loss obtained by IGOA is 19.4 MW, which is lower than that of GOA, PSO, and GA, indicating that it can find a better scheduling scheme. IGOA converges in only 63 iterations, while the traditional GOA requires 112 iterations, representing a convergence speed improvement of approximately 43.7%. In the large-scale IEEE 118-bus system, IGOA has a computation time of 26.8 s, which is 43.2% shorter than that of the traditional GOA, meeting real-time requirements. The introduction of the elite strategy and Gaussian mutation avoids local optima and ensures stable convergence even in the high-dimensional, nonlinear, and highly constrained 118-bus system.

Taking into account the characteristics of distribution network faults during typhoon weather, the impacts of fault severity, renewable energy penetration rate, and demand response availability on system dispatching decisions are analyzed separately, as illustrated in Figure 12 below.

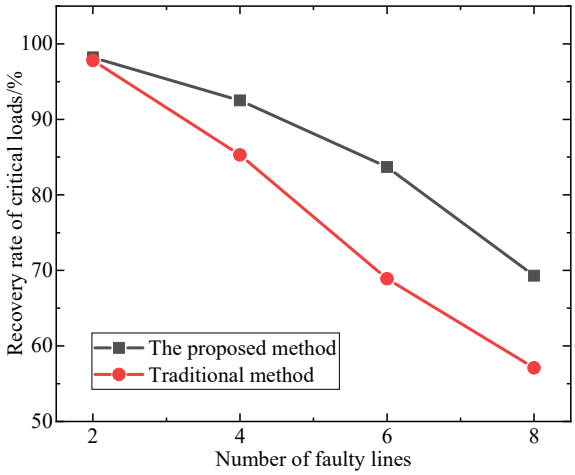

(**a**) Impacts of fault severity.

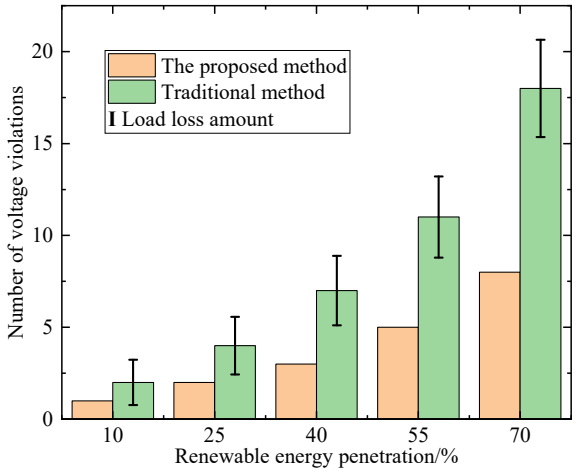

(**b**) Impacts of renewable energy penetration.

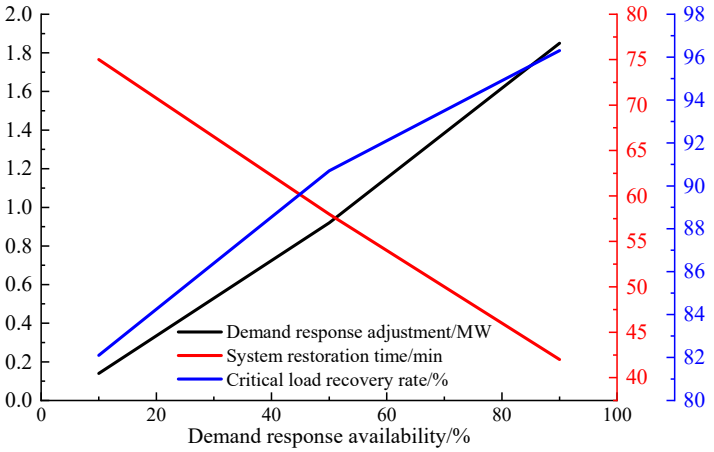

(**c**) Impacts of demand response availability.

Figure 12. Analysis of the impact of key parameters on system dispatching decisions.

As the severity of faults increases, the load restoration rates of both methods decline, but the proposed method in this paper experiences a smaller decrease. Even under severe fault scenarios, the restoration rate remains above 80%, significantly higher than that of traditional methods. This indicates that the proposed method exhibits strong robustness across varying degrees of fault severity and can effectively cope with extreme fault impacts. With the rise in renewable energy penetration, system voltage fluctuations intensify, leading to an increase in both the number of voltage violations and load losses. However, the indicators of the proposed method consistently outperform those of traditional methods. Even in scenarios with an extremely high penetration rate of 70%, the number of voltage violations is only 8, and load losses are controlled at 2.65 MW, far lower than the 18 violations and 3.8 MW load losses observed with traditional methods. This demonstrates that the proposed method can adapt to scenarios with different levels of renewable energy penetration, exhibits strong robustness, and can effectively handle power fluctuations caused by high renewable energy penetration. The higher the availability of demand response, the better the restoration performance and the shorter the restoration time achieved by the proposed method, along with a higher restoration rate for critical loads. Even in scenarios with a high unavailability rate of demand response, the proposed method can still achieve an 82.1% restoration rate for critical loads and control restoration time within 75 min. This indicates that the proposed method demonstrates strong robustness under varying conditions of demand response availability and offers broader adaptability.

6. Conclusions

Against the backdrop of increasing renewable energy penetration and the resulting complexity in modern power grid structures, power systems are confronted with considerable difficulties in maintaining economical and stable operation, particularly when subjected to extreme weather events such as typhoons. This paper presents a dedicated fast self-healing recovery scheme designed for typhoon-affected distribution networks. By taking into account the economic operation objectives of the power system as well as the physical and operational constraints on both the generation and load sides, the proposed strategy systematically integrates critical factors that affect the resilience performance of power systems. The adoption of an enhanced grasshopper optimization algorithm represents a key technical contribution, supporting efficient and prompt decision-making that is vital for realizing timely self-healing actions during grid faults. Case studies conducted on a modified IEEE 33-bus test system effectively verify the practicability and effectiveness of the presented method. The proposed approach not only strengthens the fault resistance and recovery capability of power systems against typhoon-induced disruptions but also offers meaningful guidance for the resilience enhancement of power grids under comparable extreme weather events. In general, this study provides significant insights into power system recovery and resilience improvement, presenting a feasible and high-efficiency solution to support secure and reliable grid operation amid growing operational challenges. According to the analysis, the proposed method can reduce load loss by more than 70%. Meanwhile, compared with the traditional GOA, the computational efficiency of the proposed method is improved by 45.9%.

Communication failures interact significantly with physical grid restoration. Information interruption severely impairs real-time perception, remote control and coordinated decision-making in the self-healing process of distribution networks. Without reliable communication, fault isolation, network reconfiguration and load transfer cannot be implemented in time, which slows down recovery speed, degrades self-healing performance and even causes misoperations. Sufficient information interaction is essential to realize rapid

and accurate self-healing of distribution networks. This influence also represents a direction for our future research. This influence also represents a direction for our future research.

Author Contributions: Conceptualization, Y.Z., G.C. and L.G.; software, Y.Z., G.C. and L.G.; validation, Y.Z., G.C. and L.G.; formal analysis, K.L. and S.Z.; investigation, K.L. and S.Z.; resources, K.L. and S.Z.; data curation, K.L. and S.Z.; writing—original draft preparation, Y.Z., G.C., L.G., K.L. and S.Z.; writing—review and editing, Y.Z., G.C., L.G., K.L. and S.Z. All authors have read and agreed to the published version of the manuscript.

Funding: This work was supported by the Science and Technology Project of Guangdong Power Grid Co., Ltd.: Research and Application of a Lightweight Pre-assembled Mobile Commissioning, Operation, and Maintenance Base, Project Number: 030700KC23070013 (GDKJXM20230784).

Data Availability Statement: The original contributions presented in this study are included in the article. Further inquiries can be directed to the corresponding author.

Conflicts of Interest: Authors Yanjing Zhang, Gang Chen, Liang Guo were employed by the China Southern Power Grid. The remaining authors declare that the research was conducted in the absence of any commercial or financial relationships that could be construed as a potential conflict of interest. The authors declare that this study received funding from Guangdong Power Grid Co., Ltd. The funder was not involved in the study design, collection, analysis, interpretation of data, the writing of this article or the decision to submit it for publication.

Appendix A

In the power–transportation coupled network, the distribution network (DN) model can be represented as $\Theta_{DN} = (N^{DN}, L^{DN}, N_{CS}^{DN})$. Here, N^{DN}, L^{DN} and N_{CS}^{DN} represent the sets of DN nodes, DN lines, and charging station nodes on the DN side, respectively. In this paper, the DN node loads and wind turbine outputs are considered as random uncertainty factors. Extreme events cause line disconnections, resulting in power outages at some DN nodes due to insufficient power supply. The operation of the distribution network reconfiguration model should satisfy the following constraints:

$$a_{ij,t} = \begin{cases} 0, \forall (i,j) \in L^{DN,off}, \forall t \in T \\ 1, \forall (i,j) \in L^{DN} \backslash (L^{DN,off}, L^{DN,switch}), \forall t \in T \end{cases} \tag{A1}$$

$$\sum_{(i,j)\in L^{DN}} a_{ij,t} = N^{DN} - \sum_{n^{dn}\in N_{source}^{DN}} \gamma_{n^{dn},t}, \forall t \in T \tag{A2}$$

$$\sum_{i\in\rho(j)} f_{ij,t} - \sum_{k\in\phi(j)} f_{jk,t} = 1, \forall j \in N^{DN}/N_{source}^{DN}, \forall t \in T \tag{A3}$$

$$\sum_{i\in\rho(n^{dn})} f_{i,n^{dn},t} - \sum_{j\in\phi(n^{dn})} f_{n^{dn},j,t} \le M\gamma_{n^{dn},t} + 1, \forall n^{dn} \in N_{source}^{DN}, \forall t \in T \tag{A4}$$

$$\sum_{i\in\rho(n^{dn})} f_{i,n^{dn},t} - \sum_{j\in\phi(n^{dn})} f_{n^{dn},j,t} \ge -M\gamma_{n^{dn},t} + 1, \forall n^{dn} \in N_{source}^{DN}, \forall t \in T \tag{A5}$$

$$-Ma_{ij,t} \le f_{ij,t} \le Ma_{ij,t}, \forall (i,j) \in L^{DN}, \forall t \in T \tag{A6}$$

Here, L^{DN}, $L^{DN,off}$, $L^{DN,switch}$ and N_{source}^{DN} represent the sets of DN lines, damaged lines, lines equipped with tie switches, and source nodes in the DN, respectively; $\rho(\bullet)$ and $\phi(\bullet)$ denote the sets of parent nodes and child nodes, respectively; $a_{ij,t}$ indicates the connection status of DN line (i,j) at time t, which is 1 if connected and 0 if disconnected; N^{DN} represents the number of DN nodes; $\gamma_{n^{dn},t}$ is a binary variable that equals 1 if node n^{dn} in the DN is a source node at time t, and 0 otherwise; $f_{ij,t}$ denotes the virtual power flow into DN node j at time t; and M is a large constant. Constraint (A1) sets the status of DN lines; constraint (A2) is the radial constraint of the distribution network; constraints (A3)–(A6)

describe the virtual power flow balance constraints in the DN. In a distribution network, a parent node can be understood as the source of energy or information transmission, such as a superior substation or main feeder node, which delivers electric energy or information to child nodes at the next level. Child nodes act as the receiving parties, such as lower branch line nodes or user-side nodes. Through this hierarchical relationship, reasonable power distribution and orderly information transmission are realized.

On the other hand, constraints (32)–(42) construct the optimal power flow model for the DN:

$$\sum_{i\in\rho(j)} P_{ij,t}^{DN} + P_{j,t}^{DG} + P_{j,t}^{WT} + P_{j,t}^{MESS} + P_{j,t}^{LS} = \sum_{k\in\phi(j)} P_{jk,t}^{DN} + P_{j,t}^{ED}, \forall j \in N^{DN}, \forall t \in T \quad \text{(A7)}$$

$$\sum_{i\in\rho(j)} Q_{ij,t}^{DN} + Q_{j,t}^{DG} + Q_{j,t}^{WT} + Q_{j,t}^{MESS} + Q_{j,t}^{LS} = \sum_{k\in\phi(j)} Q_{jk,t}^{DN} + Q_{j,t}^{ED}, \forall j \in N^{DN}, \forall t \in T \quad \text{(A8)}$$

$$P_{j,t}^{MESS} = \sum_{m\in M} u_{m,j,t}^{nd}(P_{m,t}^{mess,d} - P_{m,t}^{mess,c}), \forall j \in N_{CS}^{DN}, \forall t \in T \quad \text{(A9)}$$

$$Q_{j,t}^{MESS} = \sum_{m\in M} u_{m,j,t}^{nd} Q_{m,t}^{mess}, \forall j \in N_{CS}^{DN}, \forall t \in T \quad \text{(A10)}$$

$$P_{j,t}^{MESS} = Q_{j,t}^{MESS} = 0, \forall j \in N^{TN} \backslash N_{CS}^{DN}, \forall t \in T \quad \text{(A11)}$$

$$-a_{ij,t}\overline{P}_{ij}^{DN} \le P_{ij,t}^{DN} \le a_{ij,t}\overline{P}_{ij}^{DN}, \forall (i,j) \in L^{DN}, \forall t \in T \quad \text{(A12)}$$

$$-a_{ij,t}\overline{Q}_{ij}^{DN} \le Q_{ij,t}^{DN} \le a_{ij,t}\overline{Q}_{ij}^{DN}, \forall (i,j) \in L^{DN}, \forall t \in T \quad \text{(A13)}$$

$$(P_{ij,t}^{DN})^2 + (Q_{ij,t}^{DN})^2 \le a_{ij,t} \bullet \overline{S}_{ij}, \forall (i,j) \in L^{DN}, \forall t \in T \quad \text{(A14)}$$

$$U_{i,t}^2 - U_{j,t}^2 \le (1 - a_{ij,t})M + 2(r_{ij}P_{ij,t}^{DN} + x_{ij}Q_{ij,t}^{DN}), \forall (i,j) \in L^{DN}, \forall t \in T \quad \text{(A15)}$$

$$U_{i,t}^2 - U_{j,t}^2 \ge (a_{ij,t} - 1)M + 2(r_{ij}P_{ij,t}^{DN} + x_{ij}Q_{ij,t}^{DN}), \forall (i,j) \in L^{DN}, \forall t \in T \quad \text{(A16)}$$

$$\underline{U}_{j,t}^2 \le U_{j,t}^2 \le \overline{U}_{j,t}^2, \forall (i,j) \in L^{DN}, \forall t \in T \quad \text{(A17)}$$

Here, $P_{j,t}^{WT}$ and $Q_{j,t}^{WT}$ represent the active and reactive power outputs of the wind turbine, respectively; $P_{j,t}^{ED}$ and $Q_{j,t}^{ED}$ denote the active and reactive power load demands at node j, respectively; $\overline{P}_{ij}^{DN}$ and $\overline{Q}_{ij}^{DN}$ are the maximum active and reactive power values for line (i,j), respectively; $\overline{S}_{ij}$ represents the upper capacity limit of DN line (i,j); r_{ij} and x_{ij} are the resistance and reactance values of DN line (i,j), respectively; and $\overline{U}_{j,t}^2$ and $\underline{U}_{j,t}^2$ denote the lower and upper limits of the squared voltage value at DN node j at time t, respectively. Constraints (A7) and (A8) describe the active and reactive power balance in DN lines; constraints (A9)–(A11) impose power constraints on the MESS during charging (or discharging) at charging station nodes; constraints (A12) and (A13) limit the active and reactive power flowing through DN lines; constraint (A14) restricts the thermal capacity of line (i,j); and constraints (A15)–(A17) describe the voltage relationships between adjacent nodes in the DN.

The load-side response considered in this paper refers to adjustable loads, which respond to system dispatch commands. To avoid affecting the user-side power consumption experience, the adjustable range of load power is set to 95–105%, as shown in (A18) below.

$$0.95P_{i,t,o}^{load} \le P_{i,t}^{load} \le 1.05P_{i,t,o}^{load} \quad \text{(A18)}$$

Here, $P_{i,t,o}^{load}$ represents the initial power of load node i at time t. During the process of distribution network fault restoration, certain dynamic constraints must also be taken

into account. Under emergency conditions, the node voltage recovery rate should not exceed 0.02 per unit per minute to prevent voltage surges or drops that could damage equipment and ensure a stable power supply to loads. In the initial stage of restoration, the voltage range is relaxed to accommodate post-fault fluctuations; once stability is achieved, the constraints are tightened to comply with distribution network operational standards. The time difference between the operation of upper- and lower-level protection devices should be no less than 0.3 s to prevent maloperation or failure to operate, ensuring precise isolation of the faulted area. Reclosing operations should be performed more than 0.5 s after fault isolation to prevent reclosing onto permanent faults and reduce secondary damage to equipment. During island operation, the system frequency should be maintained between 49.5 and 50.5 Hz, with frequency stability achieved by adjusting renewable energy output to ensure normal equipment operation. The total renewable energy capacity within the island should be no less than 1.2 times the maximum load capacity of the area, with reserve capacity reserved to cope with load fluctuations.

References

1. Xiang, Y.; Wang, T.; Wang, Z. Framework for Preventive Control of Power Systems to Defend Against Extreme Events. *CSEE J. Power Energy Syst.* **2024**, *10*, 856–870. [CrossRef]
2. Barać, B.; Venkatasubramanian, B.V.; Capuder, T.; Panteli, M. Leveraging DER Frequency Response for Enhanced Power System Resilience. *IEEE Trans. Smart Grid* **2026**, *17*, 1359–1370. [CrossRef]
3. Huang, H.; Poor, H.V.; Davis, K.R.; Overbye, T.J.; Layton, A.; Goulart, A.E.; Zonouz, S. Toward Resilient Modern Power Systems: From Single-Domain to Cross-Domain Resilience Enhancement. *Proc. IEEE* **2024**, *112*, 365–398. [CrossRef]
4. Xin, Z.; Li, G.; Zhang, L.; Liu, D.; Bie, Z.; Luo, W.; Peng, Q.; Hao, X.; Zhang, W.; Wu, Z. Rapid Distribution System Resilience and Component Importance Assessment Based on Analytical Method. *IEEE Trans. Ind. Appl.* **2025**, *61*, 5767–5779. [CrossRef]
5. Sadeghian, O.; Mohammadi-Ivatloo, B.; Abapour, M.; Aghaei, J. Proactive Resilience-Focused Operation of Power System Against Random and Intelligent Attacks. *IEEE Access* **2026**, *14*, 19224–19248. [CrossRef]
6. Wang, Y.; Liu, H.; Wu, X.; Liu, J.; Pan, L.; Meng, F.; Shahidehpour, M. Resilience-Constrained Economic Dispatch With Graph Convolutional Network. *IEEE Trans. Power Syst.* **2026**, *41*, 142–155. [CrossRef]
7. Yin, H.; Liu, D.; Weng, J. Hierarchical Dispatch of Multi-Type Virtual Power Plants for Enhancing Resilience of Power Systems Under Wildfires. *J. Mod. Power Syst. Clean Energy* **2026**, *14*, 132–144. [CrossRef]
8. Kong, X.; Lu, Z.; Guo, X.; Zhang, J.; Li, H. Resilience Evaluation of Cyber-Physical Power System Considering Cyber Attacks. *IEEE Trans. Reliab.* **2024**, *73*, 245–256. [CrossRef]
9. Pan, W.; Shittu, E. Policies and Power Systems Resilience Under Time-Based Stochastic Process of Contingencies in Networked Microgrids. *IEEE Trans. Eng. Manag.* **2024**, *71*, 9460–9480. [CrossRef]
10. Sun, Q.; Wu, Z.; Gu, W.; Zhang, X.-P.; Lu, Y.; Liu, P.; Lu, S.; Qiu, H. Resilience Assessment for Integrated Energy System Considering Gas-Thermal Inertia and System Interdependency. *IEEE Trans. Smart Grid* **2024**, *15*, 1509–1524. [CrossRef]
11. Zhang, P.; Wang, Y.; Wang, C.; Dong, X.; Che, R.; Wu, W.; Zhang, G. Resilience Restoration Strategy for Power-Communication Coupled Networks Considering Uncertainty of Renewable Energy Output under Extreme Disasters. *IEEE Trans. Ind. Appl.* **2026**, *62*, 413–424. [CrossRef]
12. Qiu, D.; Wang, Y.; Wang, J.; Zhang, N.; Strbac, G.; Kang, C. Resilience-Oriented Coordination of Networked Microgrids: A Shapley Q-Value Learning Approach. *IEEE Trans. Power Syst.* **2024**, *39*, 3401–3416. [CrossRef]
13. Zhu, Y.; Zhou, Y.; Sun, Y.; Li, W. Fast Resilience Assessment for Power Systems Under Typhoons Based on Spatial Temporal Graphs. *IEEE Syst. J.* **2025**, *19*, 8–19. [CrossRef]
14. He, Z.; Li, Z.; Xiao, X.; Wang, C.; Ju, P. Dynamic Resilience Region-Based Proactive Scheduling for Enhancing the Power System Resilience. *IEEE Trans. Power Syst.* **2025**, *40*, 2336–2348. [CrossRef]
15. Hu, Z.; Xu, Z.; Sun, X.; Ruan, J.; Yang, X.; Qian, T.; Shi, W. Meteorological-Electrical Integrated Real-Time Resilience Assessment for Power Systems Based on Deep Learning Methods. *IEEE Trans. Smart Grid* **2025**, *16*, 3700–3713. [CrossRef]
16. Liu, W.; Wang, Y.; Shi, Q.; Yao, Q.; Wan, H. Multi-Stage Restoration Strategy to Enhance Distribution System Resilience with Improved Conditional Generative Adversarial Nets. *CSEE J. Power Energy Syst.* **2025**, *11*, 1657–1669. [CrossRef]
17. Wang, X.; Ke, J.; Wu, H.; Dong, Y.; Jiang, C.; Huang, W.; Zhang, S. A Robust Safe Reinforcement Learning Approach for Power Grid Resilience Enhancement against Typhoons via DER Flexibility Aggregation. *IEEE Trans. Ind. Appl.* **2026**, *62*, 3545–3556. [CrossRef]

18. Fu, L.; Ruan, Z.; Guo, J.; Meng, X.; Wang, X. Deepening the Understanding of Interdependence Between Higher-Order Motifs and Resilience in Power Grid Through Line Graph. *IEEE Trans. Smart Grid* **2026**, *17*, 1743–1745. [CrossRef]
19. Rong, X.; Huang, Y.; Li, G.; Bie, Z. Generative AI-Augmented Monte Carlo Simulation for Resilience Assessment of Typhoon-Affected Power Distribution Systems. *CSEE J. Power Energy Syst.* **2025**, *11*, 2659–2672. [CrossRef]
20. Zhang, D.; Li, G.; Bie, Z. An Analytical Method for Resilience Evaluation of Distribution System Based on Instantaneous Availability Increment and Probability Density Evolution. *IEEE Trans. Power Syst.* **2025**, *40*, 4452–4465. [CrossRef]
21. Kavvathas, T.E.; Konstantopoulos, G.C. Resilient Distributed Control for Power Systems With Multiple Synchronous Generators and DERs Satisfying Capability Curve Requirements. *IEEE Trans. Power Syst.* **2025**, *40*, 2994–3007. [CrossRef]
22. Khanna, K.; Govindarasu, M. Resiliency-Driven Cyber–Physical Risk Assessment and Investment Planning for Power Substations. *IEEE Trans. Control Syst. Technol.* **2024**, *32*, 1743–1754. [CrossRef]
23. Vahedi, S.; Zhao, J.; Pierre, B.J.; Wang, B.; Yusuf, J. Probabilistic Resilience-Oriented Assessment Approach for Transmission Networks Under Wildfires. *IEEE Trans. Power Syst.* **2026**, *41*, 283–295. [CrossRef]
24. Sun, S.; Li, G.; Bie, Z.; Dong, Z.Y.; Liu, J.; Chen, M.; Li, F.; Xu, M. Resilience Assessment of Power Distribution System Against Rainstorm-Induced Urban Waterlogging. *IEEE Trans. Ind. Appl.* **2025**, *61*, 7916–7928. [CrossRef]
25. Oh, B.-C.; Son, Y.-G.; Zhao, D.; Singh, C.; Kim, S.-Y. A Bi-Level Approach for Networked Microgrid Planning Considering Multiple Contingencies and Resilience. *IEEE Trans. Power Syst.* **2024**, *39*, 5620–5630. [CrossRef]
26. Zhang, B.-L.; Guo, M.-F.; Lak, M.; Lin, C.-M.; Hong, Q. Theory and Method of Distributed Virtual Zero-Sequence Synchronous Generators for Cooperative Fault Arc Suppression in Active Distribution Networks. *IEEE Trans. Ind. Electron.* **2026**, *73*, 631–645. [CrossRef]
27. Li, Z.; Liu, Z.; Zhang, X.; Feng, L. Cooperative Fault-Tolerant Control for Source-Network-Load-Storage-Based Active Distribution Network Under Communication and Actuator Faults. *IEEE Access* **2026**, *14*, 15212–15225. [CrossRef]
28. Li, Y.; Pan, Y.; Ma, M.; Wang, P. PowerCause: Leveraging Causality for Self-Recovery in Unbalanced Distribution Networks. *IEEE Trans. Reliab.* **2026**, *75*, 39–48. [CrossRef]
29. Yang, Y.; Ding, T.; Ding, Y.; Wang, S.; Zhang, X.; Li, Y.; Shahidehpour, M. Enhancing the Radiality Constraint for Multi-Period Restoration and Repair Model With Optimal Number of Islands in Active Distribution Networks. *IEEE Trans. Ind. Appl.* **2026**, *62*, 3660–3672. [CrossRef]
30. Zhang, W.; Shao, C.; Hu, B.; Xie, K.; Siano, P.; Li, M.; Cao, M. Transmission Defense Hardening Against Typhoon Disasters Under Decision-Dependent Uncertainty. *IEEE Trans. Power Syst.* **2023**, *38*, 2653–2665. [CrossRef]
31. Wang, Y.; Huang, T.; Li, X.; Tang, J.; Wu, Z.; Mo, Y.; Xue, L.; Zhou, Y.; Niu, T.; Sun, S. A Resilience Assessment Framework for Distribution Systems Under Typhoon Disasters. *IEEE Access* **2021**, *9*, 155224–155233. [CrossRef]

Disclaimer/Publisher's Note: The statements, opinions and data contained in all publications are solely those of the individual author(s) and contributor(s) and not of MDPI and/or the editor(s). MDPI and/or the editor(s) disclaim responsibility for any injury to people or property resulting from any ideas, methods, instructions or products referred to in the content.